Origins of line defects in self-reacting friction stir welds and their impact on weld quality

Judy Schneider, Professor
University of Alabama in Huntsville, Huntsville, Al 35899

Arthur C. Nunes, Jr., Weld Theoretician
NASA, Marshall Space Flight Center, Al 35812

Nomenclature

AA	aluminum alloy
AS	advancing side
Cu	copper
C-FSW	conventional friction stir welding
EDS	energy dispersive x-ray spectroscopy
FSW	friction stir welding
HAZ	heat-affected zone (of a weld)
MSFC	Marshall Space Flight Center
NASA	National Aeronautics and Space Administration
ROD	residual oxide defect
RT	Room Temperature (22°C)
RS	retreating side
SEM	scanning electron microscopy
SR-FSW	self-reacting friction stir welding
TEM	transmission electron microscopy
UTS	Ultimate Tensile Strength
V	travel velocity of the friction stir welding tool
ω	angular velocity of friction stir welding tool

Abstract

Friction stir welding (FSWing) is a solid state joining technique which reduces the occurrence of typical defects formed in fusion welds, especially of highly alloyed metals. Although the process is robust for aluminum alloys, occasional reductions in the strength of FSWs have been observed. Shortly after the NASA-MSFC implemented a variation of FSW called self-reacting (SR), low strength properties were observed. At that time, this reduction in strength was attributed to a line defect. At that time, the limited data suggested that the line defect was related to the accumulation of native oxides that form on the weld lands and faying surfaces. Through a series of improved cleaning methods, tool redesign, and process parameter modifications, the reduction in the strength of the SR-FSWs was eliminated. As more data has been collected, the occasional reduction in the strength of SR-FSW still occurs. These occasional reductions indicate a need to reexamine the underlying causes.

This study builds off a series of self reacting (SR)-FSWs that were made in 3 different thickness panels of AA2219 (0.95, 1.27 and 1.56 cm) at 2 different weld pitches. A bead on plate SR-FSW was also made in the 1.56 cm thick panel to understand the contribution of the former faying surfaces. Copper tracer studies were used to understand the flow lines associated with the weld tool used. The quality of the SR-FSWs was evaluated from tensile testing at room temperature. Reductions in the tensile strength were observed in some weldments, primarily at higher weld pitch or tool rotations.

This study explores possible correlations between line defects and the reduction of strength in SR-FSWs. Results from this study will assist in a better understand of the mechanisms responsible for reduced tensile strength and provide methodology for minimizing their occurrence.

I. Introduction

I-1   *Joint line indications*

When weld strength is reduced in FSWing, the seam trace is investigated for clues since the actual solid state joining takes place between the faying surfaces which form the weld seam. Aluminum and its alloys are known to form a native, protective oxide on the surface. It is reported that if these native surface oxides are not sufficiently broken up during the FSW process, they remain in the FSW interior, resulting in a weakened bond strength. This type of linear indication has been referred to as a lazy "S", lazy "Z", joint line defect, kissing bond, or residual oxide defect[1-9]. Inadequate dispersion of the native oxide remaining in the weld nugget was initially identified as the cause of the "joint line remnant" shown in Figure 1. The joint line remnant was believed to be comprised of an array of oxides observed in the macrostructure at very low magnifications. Typically this correlation was made by anodizing the faying surfaces and inspecting the macrograph[9]. No detailed microscopy or elemental analysis was reported in these early studies[6-9]. Ultimately these linear indications were mitigated by modification of the process parameters, such as increased tool rotation rate, which causes a finer breakup of the native oxide particles[9].

| (a) | (b) |
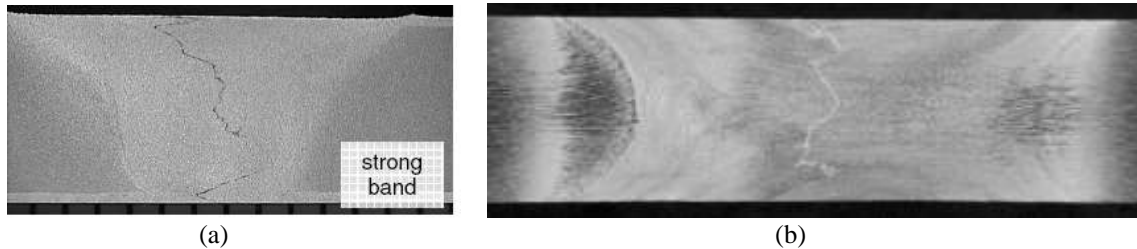
Figure 1. Metallographic images (a) of a C-FSW[10] and (b) a SR- FSW showing a typical joint line remnant feature[9]. The faying surfaces of the panels shown in the macrograph in (b) were anodized prior to the SR-FSW process.

Models of the C-FSW process have promoted the understanding that the joint is formed as the rotation of the pin surface shears the metal thereby exposing fresh un-oxidized surfaces which bond under the resulting load as the tool advances[11, 12]. The resulting fragmented Al_2O_3 particles are theorized to flow collectively during the FSW process and, if of sufficient size, accumulate in the lazy S feature reported. Since the amount of material flow increasingly varies from the root to the crown in C-FSW, most remaining oxide particles are expected to be near the root region[13]. Offsetting the pin to the retreating side (RS) is expected to reduce the size of the oxide to the point of no detection[12] due to the increasing amount of shearing strain.

Studies on AA2xxx series alloys have also reported agglomeration of Al_2Cu particles within the weld nugget. Cao and Kou[14] did a study on the agglomeration of Al_2Cu particles in a C-FSW nugget, and found they tended to form near the former weld seam and near the weld tool. Reynolds, et al.,[15] reported that the agglomeration of particles in the wake of the weld in AA2024 is responsible for the banding features observed. Sherman[16] reported on additional studies of Al_2Cu agglomeration in AA219 and found that the extent of agglomeration tended to increase as the ratio of travel velocity (V) to tool rotation (ω) decreased. The agglomeration was observed near the tool threads and on the root side of a C-FSW with porosity present in the Cu rich region.

There are very few detailed metallurgical studies in the literature on particles present in the FSW nugget. In a study by Sato[13], TEM studies of the particles along the remnant line were found to be amorphous Al_2O_3. This indicated that the oxides were not subjected to high temperatures for any length of time. Because of the amorphous nature, the oxides were attributed to native oxide films on the aluminum surfaces prior to the FSW. Findings in a study by Li et al. [1] contrast the results of Sato[13] and reported the presence of coarsened precipitates of Al_2Cu in the region around a kissing bond defect. Thus this study suggested higher temperatures occurred resulting in the coarsening. No information was provided on identification of any oxide phases present.

Most studies indicate that the joint line remnant can be eliminated by proper selection of FSW parameters of tool rotation, travel, and tilt[1, 4, 9, 17, 18]. In many studies, the remnant line was only visible when the workpiece surfaces were anodized prior to either the SR or C-FSW[3, 9]. Thus these studies indicate that the joint line remnant is

not an indication of inadequate cleaning or extended delay between pre-weld cleaning and the FSW, but rather an indication of non-optimized FSW parameters.

I-2   *Aluminum Oxidation*

Most theories and studies which regard the oxidation of solid aluminum, consider the first monolayer of oxidation to be virtually instantaneous, and only dependent on the arrival rate of oxygen. This monolayer develops into an amorphous layer whose rate of oxidation is dependent upon both the oxygen arrival rate and the rate of diffusion through the existing oxide layer. Earlier studies published the stable oxide layer at thickness of 2-3 nm[19-21]. Later studies found that the crystalline structure and orientation[22] affected the oxidation rate expanding the thickness range from 0.5 nm[22] to 4 nm[23].

The rate of oxidation for aluminum is reported to be influenced by both temperature and moisture[24]. The kinetics of aluminum oxidation follows a parabolic law in the temperature range 350 to 475ºC, reaching an equilibrium thickness rapidly. At low temperatures (<300º C) the oxide film growth rate is considered to be very fast initially, followed by an abrupt and drastic reduction to virtually zero, or self-limiting, within less than 250 s[25, 26]. At higher temperatures (> 500º C), the oxidation rate changes to linear and the oxide layer can reach a greater thickness which stabilizes at approximately 200 nm[25, 26]. The native oxide layer is amorphous, but can crystallize at elevated temperatures[22]. The kinetic rate is reduced as the oxide layer changes from amorphous to crystalline.

Based on a review of the literature, the concern regarding initial oxidation films on the workpiece would not be expected to be affected by delays between cleaning and FSWing. The initial stable oxide layer would not be expected to increase in thickness as a function of additional time at room temperature. As a stable oxide layer of 1-2 nm is noted to form within 250 s, any delays between cleaning and welding would not be expected to result in thicker oxide layers. Even in the presence of high humidity, a stable layer is still expected to form within seconds. However the noted change in oxidization rates at temperatures greater than 500ºC, suggest that the linear indications have no correlation with the native oxides on the surface of the aluminum workpiece prior to welding, but instead occur during the FSW process. Thus the occurrence of joint line remnants or line indications may correlate with FSW temperature due to weld parameters as they influence the FSW temperature and resulting weld microstructure[13, 14].

Rather than considering the native oxide responsible for internal oxidation within a FSW, it is possible that the heated material is oxidized during the FSW process. Krishnan[11] commented on the report of oxides in a manuscript by Larsson[29] and speculated that oxides could form along the layers of metal as they are sheared and consolidated in the wake of an aluminum alloy FSW. Speculation was made that at some point, purge gases might be required to avoid oxidation. Since then various studies have investigated the effect of the joint line remnant on mechanical properties and have found no detrimental effect in C-FSWs[1-5, 13].

Another source of in process oxidation could be related to the heat zone around the root and shoulder crown. If the foot print of this heat zone is larger than the foot print of the shoulder, it could experience increased oxidation in advance of the weld tool which could be stirred into the weld nugget.

I-3   *Aluminum alloy 2219*

The elemental composition of aluminum alloy 2219 is summarized in Table I[30]. It can be represented by the Al-Cu binary phase diagram shown in Figure 2 with the dashed line representing the elemental composition of AA2219. The alloy is age hardened with the precipitation sequence given in eq. (1). After a solutionizing heat treatment, the GPI and II phases precipitate out to strengthen the alloy. θ is the equilibrium phase and has the elemental composition of Al_2Cu. As can be observed from the phase diagram, 2219 will have some excess θ phase since its elemental composition range is higher than the maximum solubility. Due to the elemental range acceptable for Cu in 2219, the excess θ could vary.

Table I. Elemental composition of AA2219[30].

Aluminum, Al	91.5 - 93.8 %
Copper, Cu	5.8 - 6.8 %
Iron, Fe	<= 0.30 %
Magnesium, Mg	<= 0.02 %
Manganese, Mn	0.20 - 0.40 %
Other, each	<= 0.05 %
Other, total	<= 0.15 %
Silicon, Si	<= 0.20 %
Titanium, Ti	0.02 - 0.10 %
Vanadium, V	0.05 - 0.15 %
Zinc, Zn	<= 0.10 %
Zirconium, Zr	0.10 - 0.25 %
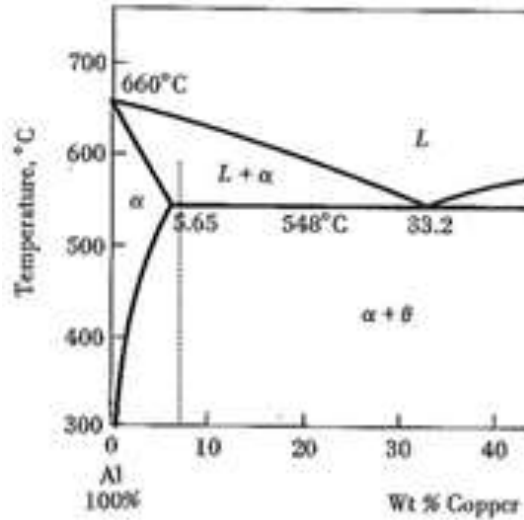
Figure 2. Binary phase diagram for Al-Cu.
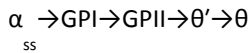
$$\alpha_{ss} \rightarrow GPI \rightarrow GPII \rightarrow \theta' \rightarrow \theta \qquad \text{[eq. 1]}$$

II.   Experimental Procedures

This study builds off a series of SR-FSWs made in 3 different thicknesses of panels of AA2219-T87 that were nominally 10 cm wide by 61 cm long. Panel thicknesses used were 0.95, 1.27, and 1.59 cm. All welds were made in the butt weld configuration using the ESAB LEGIO machine at the NASA-Marshall Space Flight Center operated in load control. An additional bead on plate (BOP) weldment was made in the 1.59 cm thick panel to evaluate the effect of the weld seam. The BOP on plate weld length was shorter as 3 weld pitches were used on one panel; therefore the overall weld length of approximately 18 cm long was lower than the butt welded configurations. A threaded pin with 3 flats was used with scrolled shoulders. All panels were stitch tacked prior to the SR-FSW process using a conventional FSW tool with a shortened pin.

The weld parameters are summarized in Table II along with the logged torque for the shoulder and the pin. The LEGIO configuration independently drives the upper shoulder from the pin and lower shoulder. Thus there is a separate torque measurement associated with the upper shoulder, and another torque measurement associated with the pin and lower shoulder. Because of the combined drive of the pin and the lower shoulder, the pin/lower shoulder torque has a higher value.

Nominally 3 specimens were removed from each weld panel and metallographically prepared to view the transverse section. The specimens were taken from the beginning section of the weld and designated M01, the middle of the weld and designated M02, and the end of the weld and designated M03. The specimens were mounted in a phenolic, ground, polished, and etched using Keller's to reveal the macrostructure.

Macrographs were made of the etched and polished specimens using a Nikon digital camera with a macro lens. Optical microscopy with a Leica was used to obtain bright field and dark field montages.   Higher magnification images were made using an environmental, field emission (FE) FEI Quanta 600 scanning electron

microscope (SEM) operated at 8 and 15 keV and configured with an energy dispersive spectrometer (EDS) operated at 15 keV. SEM images were obtained using the backscatter detector (BSI).

A total of 6 specimens were tested at room temperature for each of the 6 panels per material thickness in addition to the BOP. The tensile tests were conducted in displacement control at a rate of 0.127 mmpm at room temperature (RT).   Stress measurements were calculated using the load cell data and specimen cross sectional area. Strain measurements were obtained directly from the use of extensometers for the butt welds and from the cross head displacement for the BOP weld.

To evaluate the oxygen content of the SR-FSW nugget region, 3 specimens were sent out to Westmoreland Laboratories for LECO analysis in addition to the parent material. At the conclusion of the summer, this analysis has not been completed.

Evaluation of the surface material into the weld nugget was evaluated by the use of 0.15 mm thick Cu applied using a plasma spray process to the surface of 6.4mm thick 2219 panels. The Cu was plated onto either the AS crown or root surfaces as shown in Figure 3 just prior to the transition zone.   X-ray radiographs were made at the NASA-MSFC of the resulting plan and transverse views to document Cu entrainment into the weld nugget.

Table II. SR-FSW Schedule

| Panel ID	Thickness (cm)	Pinch force (kN)	Weld pitch (rev/mm)	Spindle torque (N-m)	Pin torque (N-m)
P13	0.95	0.9	0.64	113	147
P14	0.95	0.9	0.64	107	154
P15	0.95	0.9	0.64	108	154
P16	0.95	0.9	0.67	118	143
P17	0.95	0.9	0.67	125	140
P18	0.95	0.9	0.67	124	137
P01	1.27	2.2	0.73	143	265
P02	1.27	2.2	0.73	143	262
P03	1.27	2.2	0.73	145	260
P04	1.27	2.2	0.84	162	215
P05	1.27	2.2	0.84	163	213
P06	1.27	2.2	0.84	164	215
P07	1.59	2.0	0.79	170	292
P08	1.59	2.0	0.79	161	295
P09	1.59	2.0	0.79	154	301
P10	1.59	2.2	0.87	179	250
P11	1.59	2.2	0.87	162	262
P12	1.59	2.2	0.87	168	259
BOP 1	1.59	2.0	0.79	161	297
BOP 2	1.59	2.2	0.82	162	279
BOP 3	1.59	2.2	0.87	170	244
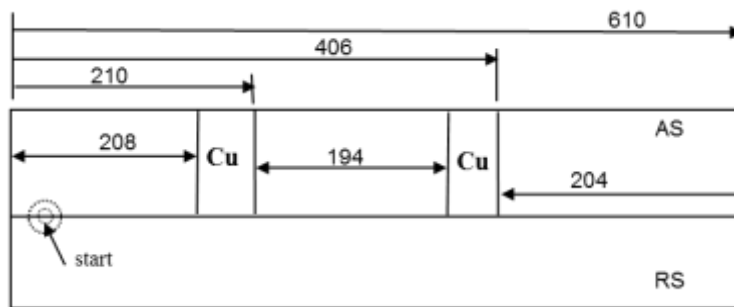
Figure 3. Configuration of weld panels with Cu plating over a 38mm wide zone. Units are in mm.

III.   Results and Discussion

III-1   Mechanical Properties

Although 3 thickness panels were welded and evaluated, only the results from the 1.59 cm thick SR-FSWs will be presented in this report. The remainder of the data is published elsewhere[31]. Figures 4 and 5 present the mechanical property data for the 1.59 cm panel thickness for the butt weld and bead on plate configurations, respectively. The strength values are normalized to the acceptance values[32]. A reference line is drawn at 100% of the design allowable for the UTS and at 10% strain for the elongation to failure plots.

Only one of the butt welded panels displayed reduced UTS and elongation to failure at the higher weld pitch. A similar reduction in strength was observed for BOP 3, which was run at the same SR-FSW process parameters as 625-P10.   Overall the differences in the properties between the butt weld and the BOP SR-FSWs could be attributed to the difference in weld length. The butt weld was 61 cm long vs the 18 cm long BOP. Both the butt weld and the BOP weld showed reduced UTS at the higher weld pitch. Thus the faying surfaces of the weld seam are not solely responsible for reduced properties.
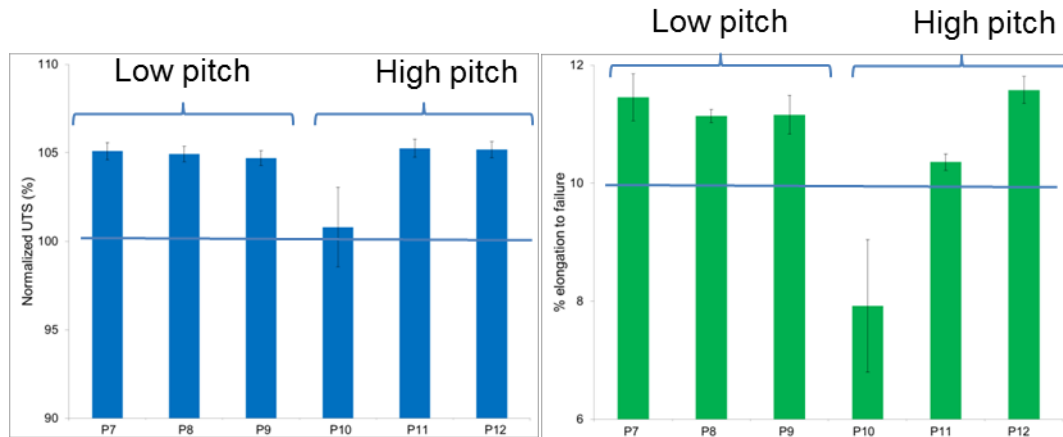

Figure 4. Summary of the normalized UTS (a) and % elongation to failure (b) of the 1.59 cm thick SR-FSW panels tested at RT.
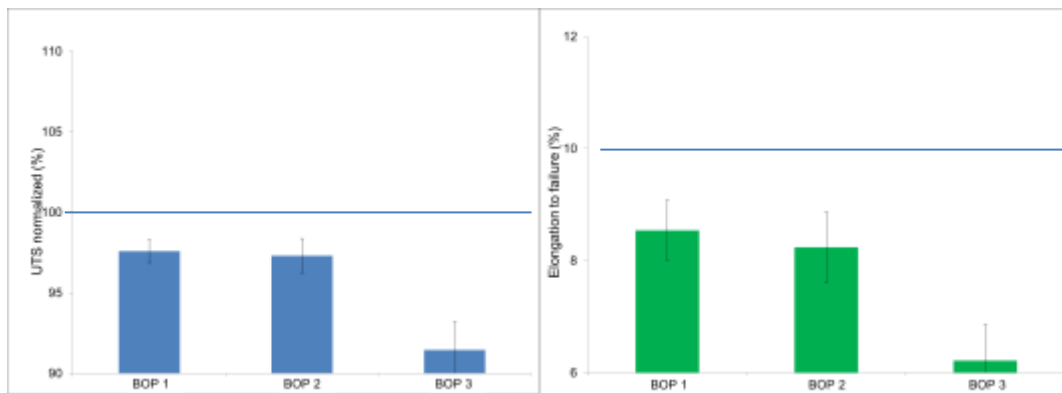

Figure 5. Summary of the normalized UTS (a) and % elongation to failure (b) of the 1.59 cm thick SR-FSW BOP panels tested at RT.

III-2   Metallographic studies

Representative specimens for metallurgical analysis were selected on the basis of nominal and lowest properties. Figure 6 and 7 present a group of images taken of specimen 625-P10, which had the lowest mechanical properties and was welded at the higher weld pitch weld in the 1.59 cm thick, butt welded panels.

An overall photograph of the transverse section of the etched weld is shown in Figure 6a. Image montages were made of the specimen in the unetched condition to show the location of line features. Montages were made of the specimen using bright field (Figure 6b) and dark field (Figure 6c). Various line features were found and are highlighted on Figure 6b and 6c. This area was marked with carbon tape and a corresponding BSI montage was made in the SEM and is shown in Figure 6d. These line features were common to all the SR-FSWs made in this study.
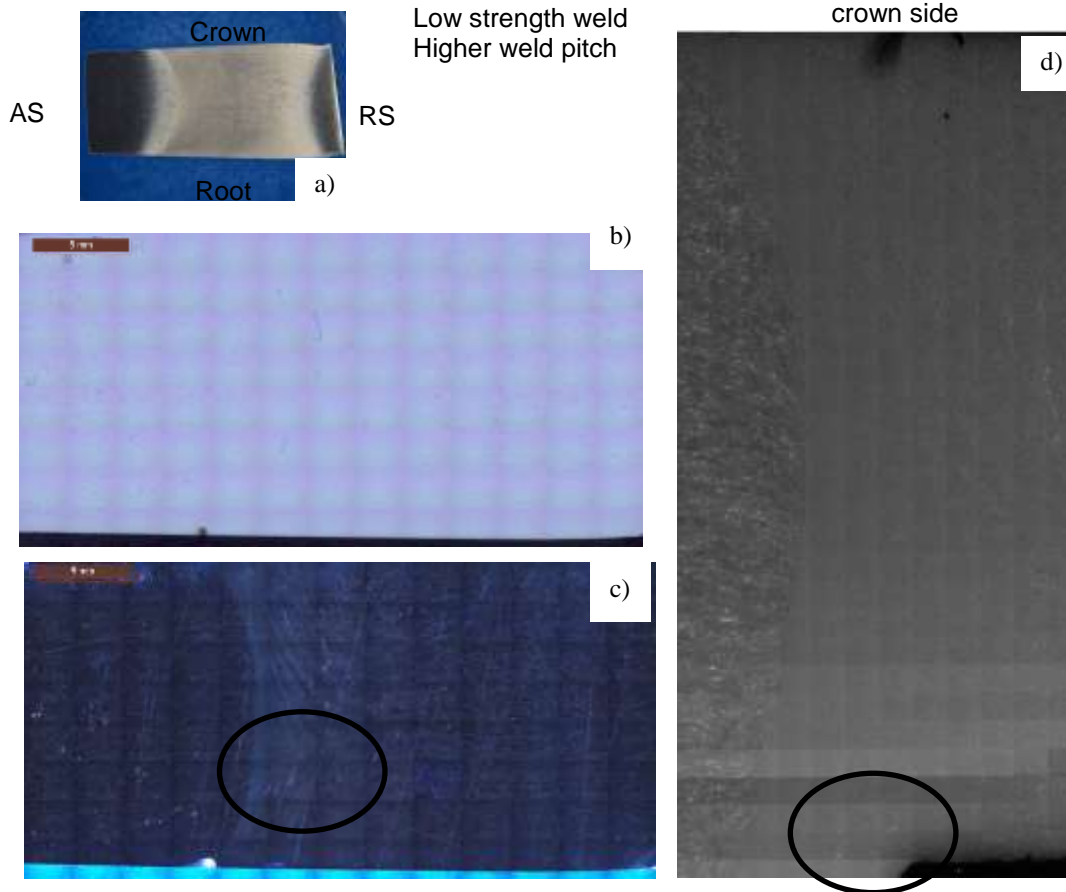
Figure 6. Optical images of the unetched metallographic of specimen 650-P10. This specimen was welded at the higher weld pitch and displayed the lowest UTS and ductility. An overall photograph of the transverse section of the weld is shown (a). Montages were made of the specimen using bright field (b) and dark field (c). Identified regions (shown in circle on (c) were imaged in the SEM and a montage is shown of this region (d).

Figure 7 shows higher magnification SEM BSI of the region of the unetched metallographic specimen circled in Figure 6d. The white regions observed are Cu rich (30 to 35 wt%). The Cu rich regions also showed slight amounts of Mn (1-2 wt%) and Fe (4 to 6 wt%). EDS analysis showed no appreciable indication of oxides present (0.5 to 0.6 wt%) in any of the regions.
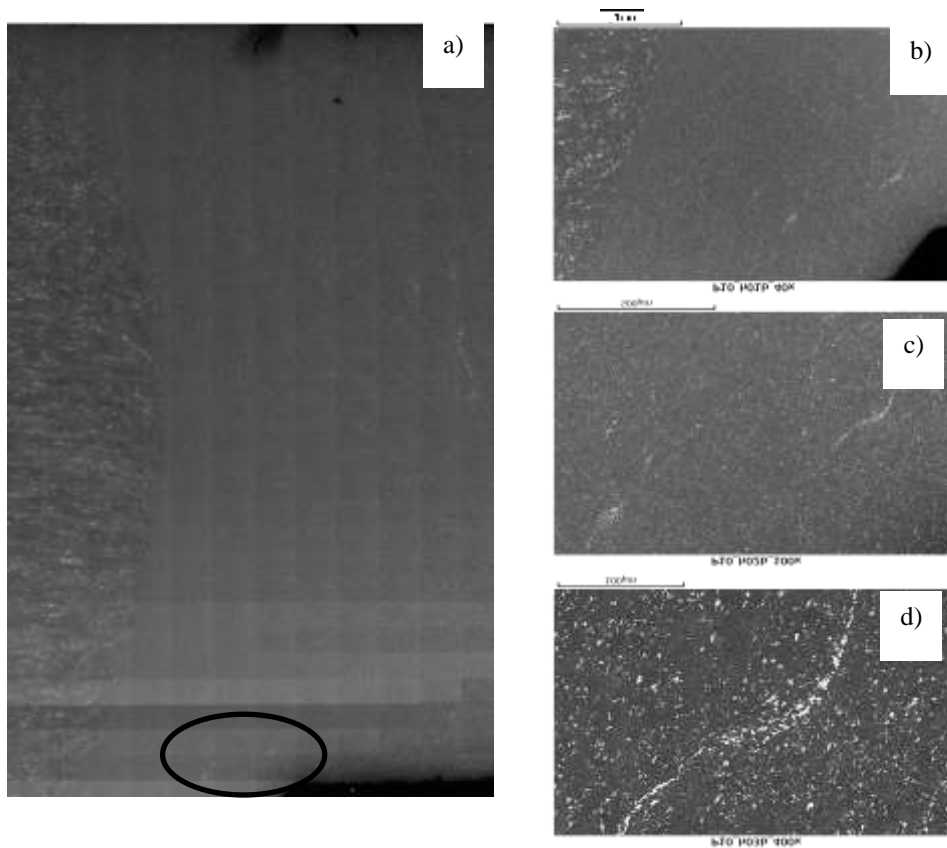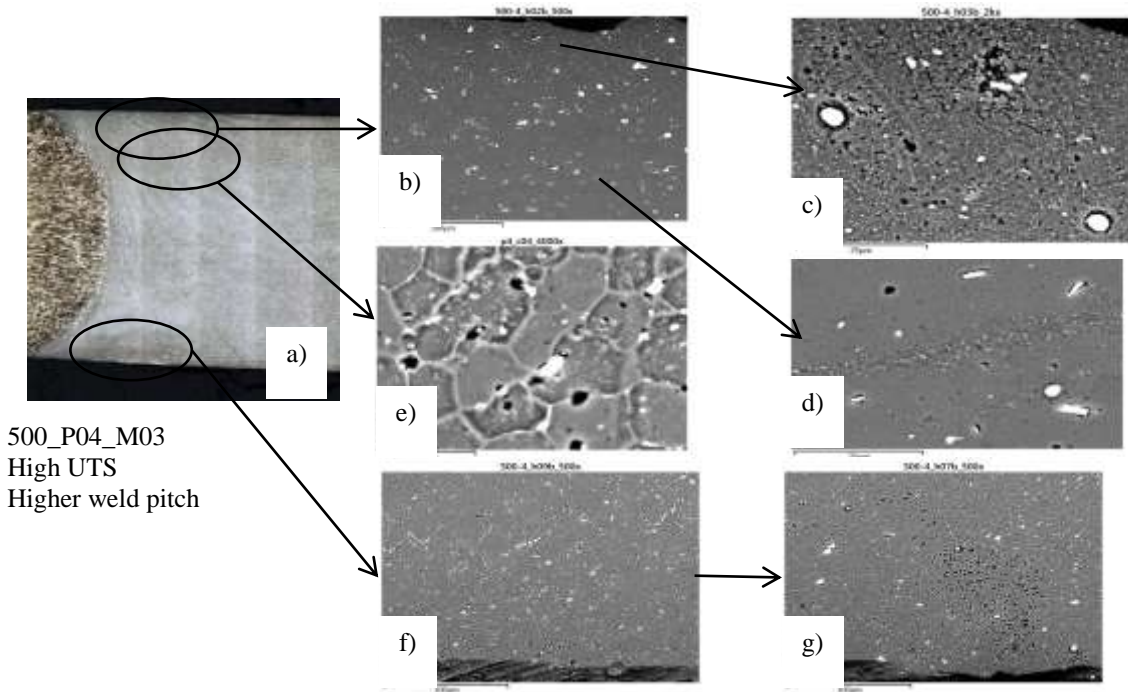
Figure 7. SEM of the unetched metallographic BS image of specimen 650-P10 (a). This specimen was welded at the higher weld pitch and displayed the lowest UTS and ductility. The white regions are Cu rich with negligible indication of oxides present. (b-d) show magnifications of the region circled in (a).
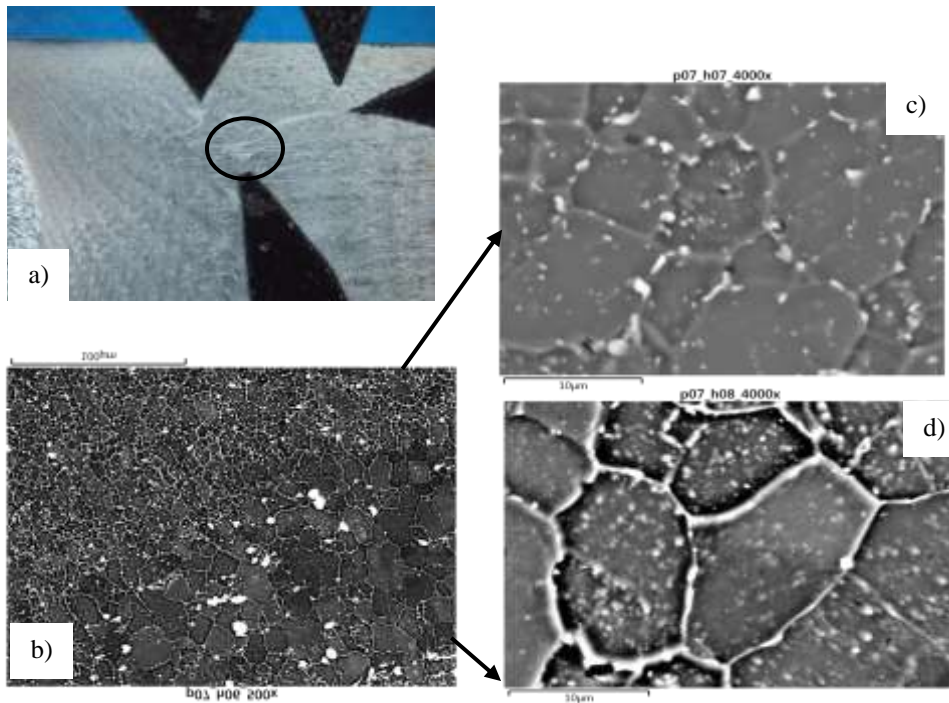
SEM-BSI for the etched metallographic specimen 500-P04 are shown in Figure 8. This specimen was welded at the higher weld pitch, but displayed nominal UTS and ductility. A range of porosity is observed at the crown (Figure 8b and 8c) and root (Figure 8f and 8g) surfaces. Pores are noted to contain Cu rich particles as shown in Figure 8e. From EDS, the Cu rich regions have 27 wt% Cu with similar levels of Mn and Fe as the Cu rich regions in Figures 6 and 7. However, this region has more oxygen (5-6 wt%) than measured in Figures 6 and 7. The base material in this region has an oxygen content of 2-3 wt% with no detectable Mn or Fe.

SEM-BSI for the etched metallographic specimen 625-P07 are shown in Figure 9. This specimen was welded at the lower weld pitch and displayed nominal UTS and ductility. An overview of the specimen in Figure 9a shows light and dark banded regions. A close up of the banded structure circled in Figure 9a is presented in Figure 9b. From this magnification, it appears that the bands correspond to "fine" and "coarse" grains. Close up of the fine grained region in Figure 9c, compared to the close up of the coarse grained region in Figure 9d, show comparable grain sizes. However in Figure 9c there appear to be more sub-boundaries present within a grain. The similar surface appearance of each grain in this etched specimen, suggests an overall crystallographic texture in this region. While there are Cu particles along the grain boundaries in Figure 9c, they do not appear to be continuous. In contrast, the coarse grain region in Figure 9d shows more variation on the etched grain surfaces suggesting a more random orientation of the grains. Very few sub-boundaries can be observed. In addition, the grain boundaries appear to have more continuous Cu present. Such variations within a FSW nugget have been correlated with various textures resulting from the thermo-mechanical deformation occurring during the FSW process[33, 34].

Figure 8. SEM-BSI of the etched metallographic BS image of specimen 500-P04 (a). This specimen was welded at the higher weld pitch and displayed nominal UTS and ductility. A range of porosity is observed at the root and crown surfaces (b, c, f, g). Pores are noted to contain Cu rich particles (e).


Figure 9. SEM-BSI of the etched metallographic BS image of specimen 625-P07. This specimen was welded at the lower weld pitch and displayed nominal UTS and ductility. Variations in weld texture (a) and grain boundaries (c and d) are observed within the weld nugget. A close up of the banded structure shown in (a) is presented in (b). Close up of fine grained region is shown (c) along with the coarse grained region (d).

Gratecap, et al.[35] has recently published a study on the mechanisms of band formation which are shown in Figure 10a. In this theorized mechanism, the tool oscillations force the sheared bands of metal together in the wake of the FSW. This thermo-mechanical history would be expected to be captured in the metallographic structure, especially in lower pitch welds which would correspond to lower temperatures. Higher pitch welds would be expected to anneal out these variations across the sheared metal band. Figure 10b shows an optical microscopy image of an etched cross section of typical flash formed during a FSW of 2219. A range of microstructural variations can be observed from the tool interface shearing surface to the outer free edge. This variation in microstructure would be expected from variations in temperature, strain, and strain rate in material transported during each tool rotation. Thus it is proposed that this microstructural variation across the layers of sheared material is responsible for the light and dark regions observed in the transverse metallographic images of the weld nugget. More detailed electron back scatter diffraction (EBSD) would be required to verify this hypothesis.


(a)   **(b)**
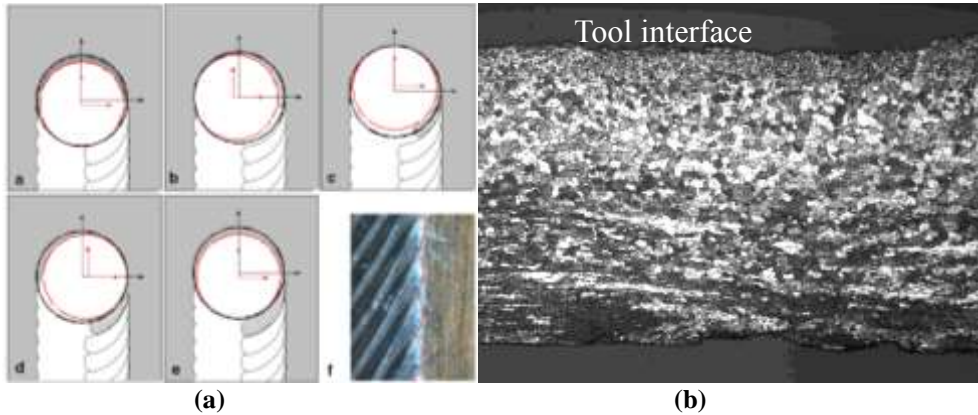
Figure 10. Gratecap's[35] mechanism of band formation during a FSW (a). Optical microscopy image of an etched cross section of typical flash formed during a FSW of 2219 (b). A range of microstructural variations can be observed from the tool interface shearing surface to the outer free edge.

Figure 11 shows additional images from specimen 625-P07 in which Cu particles are aligned within the weld nugget, presumable along shear bands from the SR-FSW process. Most noteworthy on these Cu particles are the features within them which resemble the forehead of a Klingon. The light regions have a high concentration of Cu (42-45 wt%) with 1-2 wt% of oxygen. A similar amount of Mn and Fe are noted as in the areas in Figure 7 and 8, but there now appears Sb (2-3 wt%). The lighter region surrounding the bright Cu particle has approximately 34 wt% Cu with minor 0.5 wt% oxygen and none of the trace elements (Mn, Fe, Sb). The Cu rich regions are approximately 7 μm in diameter.
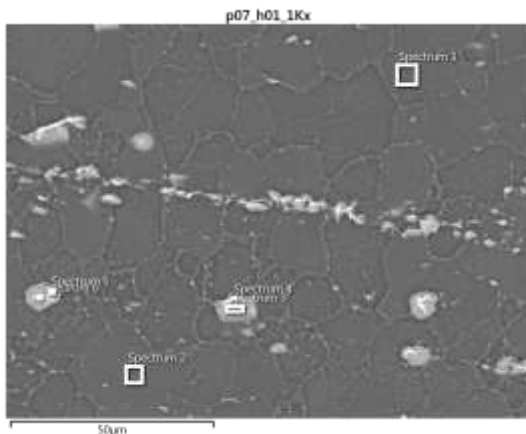
Figure 11. Cu rich bands in weld nugget of specimen 625-P07. This specimen was butt welded at the lower weld pitch in 1.59 cm thick panels.

For comparison, Figure 12 shows the Cu rich regions in the parent material used in 2015 welds vs 2016 welds. The morphology and elemental content is similar to that shown in Figure 11 for the refined Cu rich region in the FSW nugget. Figure 12b shows larger light regions which correspond to the θ phase. This area is surrounded by a slightly lower concentration of Cu which corresponds to the eutectic composition.

(a)   (b)
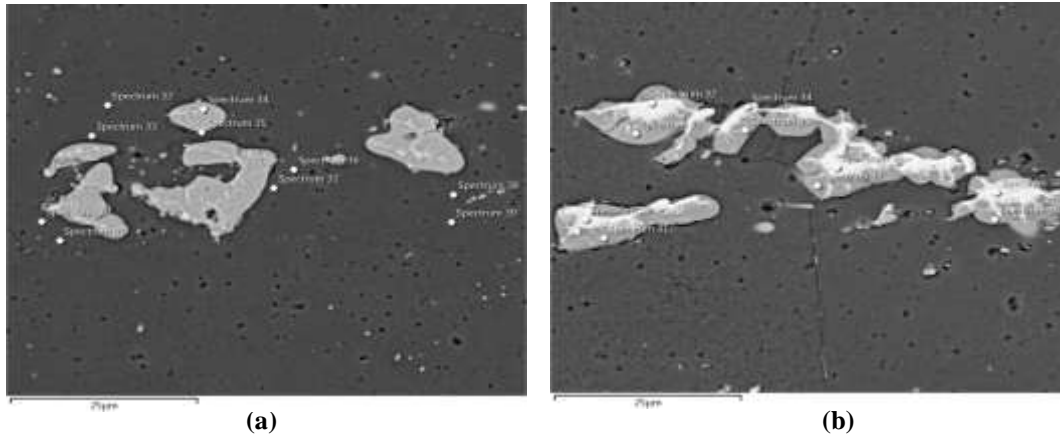
Figure 12. SEM BSI of Cu rich regions in the parent material from SR-FSWs made in 2015 with an average size of 10 μm (a) and in in 2016 with an average size of 20 x 7 μm.

Table III summarizes the elemental composition, recommended heat treatment temperatures and a summary of the expected welding temperatures for AA 2219. The range of Cu content for AA2219 of 5.8 to 6.8 wt% exceeds the solid solution composition of 5.65 wt%. Thus AA2219 is a two phase alloy comprised of α + θ phases. The recommended heat treatment is to solid solutionize at 535º C, which is just below the eutectic temperature of 548º C.

Table III. AA2219 elemental composition, eutectic temperature, heat treatment temperature, and expected welding temperature.

θ composition: Al_2Cu (54 wt% Cu)

Eutectic composition: 33 wt% Cu
Eutectic temperature: 548º C

Heat treatment:
    535º C (SS)
    175º C/18 h (age)

Welding temperature:
    0.90 Tmp = 567º C
    0.85 Tmp = 520º C
    0.80 Tmp = 473º C

The expected temperatures during a FSW process are in the range of 0.90 to 0.80 homologous temperatures. These temperatures are noted to be close to the eutectic temperature which could be easily exceeded in a weld with a higher pitch or higher RPM.

In a survey of heat treatment on aluminum alloys, noted defects are reported for 2xxx series alloys during either the solutionizing or quenching steps of heat treatments[36]. The quenching defects are primarily related to

11

cracking and distortion. However during the solutionizing step, either oxidation or incipient melting is reported. The oxidation occurs at elevated temperatures and if sufficient moisture is present, the moisture can decompose releasing hydrogen and related porosity.

Incipient melting is reported to occur when coarse particles of Al_2Cu are present. High up-quenching rates in 2xxx series alloys provide inadequate time for the Al_2Cu particles to dissolve[37]. Thus they melt if of sufficient size and the temperature exceeds that of the eutectic. Incipient melting has been reported in FSW of 2219 when Cu content was at the higher 6.31wt% end of the compositional range rather than the lower 5.83wt% end[38].

Figure 13 shows an optical metallographic image of an etched specimen which had Cu plated on the AS root surface. Minimal entrainment of the Cu into the weld nugget is observed. The Cu appears to distribute over the surface under the shoulder and highlights flow lines.


Figure 13. Optical microscopy image of an etched sample of a transverse SR-FSW made in 0.63 cm thick plates. Cu was plated on the AS root surface and is shown to have minimal entrainment into the weld nugget region.

Another source of oxygen entering the FSW is related to the temperature and the enhanced oxidation rates above 500° C. As the oxidation rate is noted to increase with increasing temperature, it is conceivable that the faying surface would be prone to increased oxidation during the FSW if exposed to entrained air. At the estimated FSW temperature of aluminum alloys (530 to 580 °C), the oxidation behavior rate changes from parabolic to linear. The literature reports that the temperature of the FSW panel has been most strongly correlated with the tool rotation[27, 28].

It is generally assumed that minimal entrained air enters the faying surface during a butt weld. However as the weld panels increase in thickness, it has been observed that gaps form along the weld seam in advance of the tool form. As this gap increases, it can provide a passage way for air to enter causing enhanced oxidation at the elevated temperatures. This would be further exasperated if the work piece material was to locally liquate at the welding temperature. Exposure to air at these temperatures would oxidize these molten regions which would tend to be located at the grain boundaries.

Additionally at higher weld pitches, the heat profile may extend outside the shoulder envelope as shown in Figure 14a. This would expose high temperature surface material to air promoting oxidation. Under lower weld pitch, the heat profile maybe kept within the shoulder envelope as shown in Figure 14b. This would reduce the potential for surface oxidation during the SR-FSW.
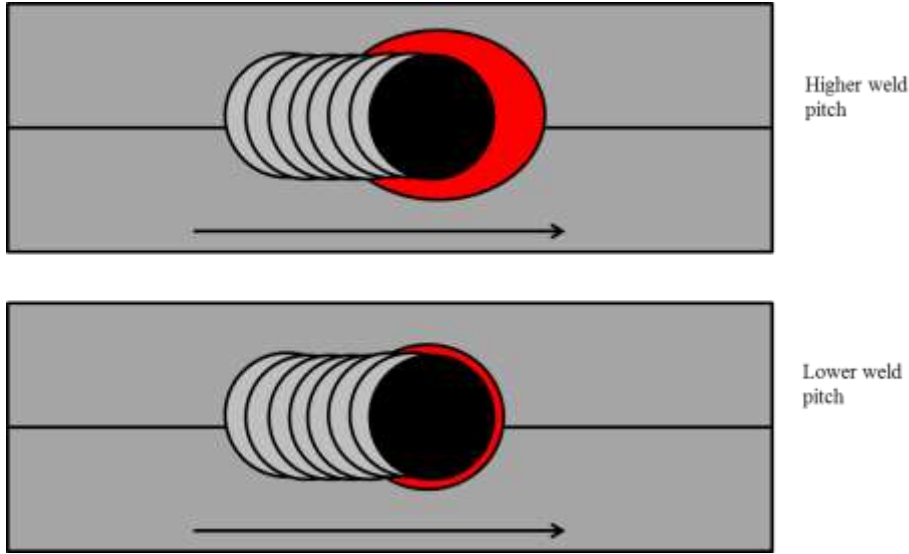
Figure 14. At higher weld pitch, the heat profile extends past the tool shoulder (a) while at lower weld pitch, it is possible to keep the heat profile within the tool shoulder envelop.

The chemical composition will also affect the resulting 2nd phases present in the panels. Cu content can vary in AA2219. With higher Cu concentrations, there would be more excess θ phase which could explain variation among different lots of AA2219 or even along the length of a weld panel. Refinement of the θ phase may also vary as a function of the initial panel thickness. As the initial panel thickness increases, it may not be possible to get sufficient work into the plate to refine the excess θ particles.

V. Summary

Studies in the literature on the remnant line defect in C-FSWs have concluded that non-optimized parameters are responsible for the reduction observed in mechanical properties. However the seemingly random occurrence of reduced strength in FSWs suggests there is another underlying cause. This study considered the effect of line features observed in FSW nuggets with the weld quality.

Oxidation is not always associated with the line features, which can be either variations in the texture or strings of Cu rich particles. Since thicker oxides require higher temperatures, in excess of 500ºC to form, these would be promoted on the interior surfaces during a FSW if exposed to entrained air especially in regions of localized liquation.

Understanding the underlying cause and effect of the presence of internal oxide within the FSW nugget would improve the robustness of the process. Possible causes include:

1)   Variations in amount of alloying elements in the workpiece.
2)   Size of initial Al_2Cu particles, possibly as a function of the initial panel thickness.
3)   Higher temperatures during SR-FSWs may promote localized liquation in the presence of coarsened Al_2Cu particles.

This study did not find a correlation between line features in metallographs of SR-FSW specimens and reduced weld strength. However, it can be concluded that if the parent material contains coarse θ particles, the up-quenching rate during the FSW process could cause localized (incipient) melting to occur.

As shown in the images presented, θ particles decorate the grain boundaries within the weld nugget. If incipient melting were to occur, the molten material would be most susceptible to oxidation at weld temperatures. The resulting solidification would leave a weakened area at the grain boundary that is difficult to find during routine metallography. Subsequent tensile testing would result in cracks forming along these weakened grain boundaries.

Thus it is not believed that the cracks observed in the metallographs of tensile specimens occurred during the welding process nor are they believed to result from native oxides on the surfaces of the weld panels. These cracks, observed post-test, are likely indications of weakened grain boundary regions. These are more prone to occur during the crown and root surfaces and can serve as fracture initiation sites.

Acknowledgments

References

[1]Li, B.. Shen, Y., and Hu, W., "The study on defects in aluminum 2219-T6 thick butt friction stir welds with the application of multiple non-destructive testing methods," *Materials and Design*, Vol. 32, , 2011, pp. 2073–2084.

[2]Chen, H-B., Yan, K., Lin, T., Chen, S-B., Jiang, C-Y., and Zhao.Y., "The investigation of typical welding defects for 5456 aluminum alloy friction stir welds," *MSEA* Vol. 433, , 2006, pp. 64–69.

[3]Klages, H. K., "The "Lazy S" feature in friction stir welding of AA2099 Aluminum-Lithium alloy," Navy Postgraduate School, Monterey, CA, MS Thesis, December 2007.

[4]Leonard, A.J., and Lockyer, S.A., "Flaws in friction stir welds," *4th Intl. Symp. FSWing*, Park City, Utah, May 14-16, 2003.

[5]Liu, H.J., Chen, Y.C., and Feng, J.C., "Effect of zigzag line on the mechanical properties of friction stir welded joints of an Al–Cu alloy," *Scripta Mat.*, Vol 55, 2006. pp. 231-234.

[6]SDS 6103 SR-FSW Reference Book, Section 2.1: FY02 SDS 3774 Phase II Friction Stir Welding: Task 1: Characterize Weld Pin Tooling for SR-FSW Process. 0.320-inch-thick 2219-T87/2195-T8M4SR-FSW 0.5-20 Left-Handed Thread Pin Extreme Weld Parameter Map and Verification Welds, Lockheed Martin.

[7]SDS 6103 SR-FSW Reference Book, Section 2.2 SDS 3774 FY02 Phase II Friction Stir Welding Task 1 Characterize Weld Pin Tooling for SR-FSW Process 0.320-inch-thick 2219-T87/2195-T8M4 SR-FSW Extreme Weld Parameter Maps and Process Envelopes, Lockheed Martin.

[8]SDS 6103 SR-FSW Reference Book, Section 3.1, SDS 3774 FY02 Phase II Friction Stir Welding Task 1 Characterize Weld Pin Tooling for the SR-FSW Process Draw Filed Weld Joint Quick Look, Lockheed Martin.

[9]SDS 6103 SR-FSW Reference Book, Section 3.2, SDS 6103 FY03 Phase II Friction Stir Welding Task 1 0.320t Weld Schedule Development Pre Weld Cleaning Method. Lockheed Martin.

[10]Private conversation with Murray Mahoney, formerly of Rocketdyne, January 2016.

[11]Krishnan, K.N., "On the formation of onion rings in friction stir welds," *MSEA*, Vol. 327, 2002, pp. 246–251.

[12]Nunes, Jr., A. C., "Metal Flow in Friction Stir Welding," Conf. Proc., MS&T, 2006.

[13]Sato, Y.S., Yamashita, F., Sugiura, Y., Park, S.H.C, and Kokawa, H., "FIB-assisted TEM study of an oxide array in the root of a friction stir welded aluminum alloy," *Scripta Mater.*, Vol. 50, 2004, pp. 365–369.

[14]Cao, G., and Kou, S., "Friction stir welding of 2219 aluminum: behavior of θ (Al2Cu) particles," *Welding J. Supp.*, 2005, pp. 1s-8s.

[15]Sutton, M.A., Yang, B., Reynolds, A.P., and Taylor, R., "Microstructural studies of friction stir welds in 2024-T3 aluminum," *MSEA*, Vol. A323, 2002, pp. 160–166.

[16]Sherman, P.S., "Investigation of agglomerated theta particle formation in 2219 aluminum," Final Report NASA SFFP, NASA-MSFC, 2006.

[17]Liu, H.J., Fujii, H., Maeda, M., and Nogi, K., "Tensile fracture location characterization of friction stir welded joints of different aluminum alloys," *J. Mater. Sci. Technol.*, Vol. 20, 2004, pp. 103–105.

[18]Kim, Y.G., Fujii, H., Tsumura, T., Komazaki, T., and Nakata, K., "Three defect types in friction stir welding of aluminum die casting alloy," *MSEA*, Vol. 415, 2006, pp. 250–254.

[19]Doherty, P.E., and Davis, R.S., "Direct Observation of the Oxidation of Aluminum Single-Crystal Surfaces," *J. Appl. Phys*., Vol. 34, 1963, pp. 619-628.

[20]Thomas, K., and Roberts, M.W., "Direct Observation in the Electron Microscope of Oxide Layers on Aluminum," *J. Appl. Phys*., Vol. 32, 1960, pp. 70-75.

[21]Steinheil, A., "Struktur und wachstum duenner obserflaechenschiechten auf metallen bei oxydation an luft," *Ann. Phys*., Vol. 19, No. 5, 1934, pp. 465-483.

[22]Trunox, M.A., Schoenitz, M., Zhu, X., and Dreizin, E.L., "Effect of polymorphic phase transformations in Al_2O_3 film on oxidation kinetics of aluminum powders," *Combustion & Flame*, Vol. 140, 2005, pp. 310-318.

[23]Sanchez-Lopez, J.C., Gonzalez-Elipe, A.R., and Fernandez, A., "Passivation of nanocrystalline Al prepared by the gas phase condensation method: an XPS study," *J. Mater. Res.*, Vol. 13, No. 3, p. 703-710, 1998.

[24]Hart, R.K., "The oxidation of aluminum in dry and humid oxygen atmospheres," Proceed. Royal Society of London, Series A. Mathematics & Physical Sciences, Vol. 236, No. 1204, 1956, pp. 68-88.

[25]Smeltzer, W.W., "Oxidation of Aluminum in the Temperature Range of 400º to 600º C," *J. Electrochemical Soc*., 1956, pp. 209-214.

[26]Jeurgens, L.P.H., Sloof, W.G., Tichelaar, F.D., and Mittemeijerc, E. J., "Growth kinetics and mechanisms of aluminum-oxide films formed by thermal oxidation of aluminum," *J. Appl. Phys.*, Vol. 92, 2002, pp. 1649.

[27]Record, J.H., Covington, J.L., Nelson, T.W., Sorensen, C.D., and Webb, B.W., "A look at statistical identification of critical process parameters in friction stir welding," *Welding J.*, Vol. 86, No. 4, 2007, pp. 97s - 103s.

[28]Schneider, J.A., Stromberg, R., Schilling, P., Cao, B., Zhou, W., Morfa, J., and Myers, O., "Processing effects on the friction stir weld stir zone," *Welding J.*, 2013, pp. 11s-19s.

[29]Larsson, H., Karlsson, L., Stoltz, S., and Bergqvist, E-L., "Joining of dissimilar Al-alloys by Friction Stir Welding," *2nd Intl. Symp. FSW*, TWI, Gothenburg, Sweden, 2000.

[30]http:\\www.matweb.com, accessed 8/10/16.

[31]Schneider, J.A., Chen, P-S., and Nunes, Jr., A.C., "Formation of oxides in the interior of friction stir welds," Session 9B, *11th Intl. Symp. FSW*, TWI, Cambridge GB, May 17-19, 2016.

[32]Fisher, M., Boeing Company Memo, #EYBF-MAF-14-029, October 16, 2014.

[33]Field, D.P., Nelson, T.W., Hovanski, Y., and Jata, K.V., "Heterogeneity of Crystallographic Texture in Friction Stir Welds of Aluminum," *MMTA*, Vol. 32, 2001, pp. 2869-2877.

[34]Schneider, J.A., and Nunes, Jr., A.C.,"Characterization of plastic flow and resulting micro textures in a friction stir weld," *MMTB*, Vol. 35, 2004, pp. 777-783.

[35]Gratecap, F., Girard, M., Marya, S., and Racineux, G., "Exploring material flow in friction stir welding: Tool eccentricity and formation of banded structures, *Intl J. Matl Forming,* Vol. 5, No. 2, 2012, pp. 99-107.

[36]MacKenzie, D.S., "Heat treating aluminum alloys for aerospace applications," *Heat Treating Progress*, 2005, pp. 36-43.

[37]Reiso, O., Overlie, H-G., and Ryun, N., "Dissolution and melting of secondary Al2Cu phase particles in an AlCu alloy," *MMTA*, Vol. 21, 1990, pp. 1689-1695.

[38]J. Kang, Z-C. Feng, G.S. Frankel, I.W. Huang, G-Q. Wang, and A-P. Wu., "Friction Stir Welding of Al Alloy 2219-T8: Part I-Evolution of Precipitates and Formation of Abnormal Al_2Cu Agglomerates," *MMTA*, Vol. 47, No. 9, 2016, pp. 4553-4565.